RESEARCH ARTICLE

nano select Open Access WILEY

Generation of Si@C/SiC@C core–shell nanoparticles by laser irradiation of silicon grinding waste

Kanon Minami[1] | **Kyosuke Kobinata**[2] | **Jiwang Yan**[3] (ORCID)

[1]School of Integrated Design Engineering, Graduate School of Science and Technology, Keio University, Yokohama, Japan

[2]Sales Engineering Department, DISCO Corporation, Tokyo, Japan

[3]Department of Mechanical Engineering, Faculty of Science and Technology, Keio University, Yokohama, Japan

Correspondence
Jiwang Yan, Department of Mechanical Engineering, Faculty of Science and Technology, Keio University, Yokohama, Japan.
Email: yan@mech.keio.ac.jp

Abstract
In recent years, the demand for lithium-ion batteries has increased because of the global focus on carbon neutrality. Silicon/carbon (Si/C) composite nanoparticles have potential for application as high-performance anode materials in lithium-ion batteries, which can enable the widespread use of lithium-ion batteries or lithium-ion capacitors and contribute toward decarbonized society. In this study, Si@C/SiC@C core–shell nanoparticles with sizes in the range of 10–40 nm were produced by pulsed laser irradiation (wavelength = 1070 nm; pulse width = 10 ms) of a mixture of graphite powder and waste Si powder discharged from the grinding process of Si wafers. High-speed camera observations of the laser-induced plume were conducted to elucidate the nanoparticle generation mechanism, and it was determined that Si/SiC nanoparticles were formed within the laser-induced plume in the early stage of laser irradiation. Si and C demonstrated different plume propagation patterns and plume decay times, and the time difference enabled the coating of the generated Si/SiC nanoparticles with a thin layer of graphene, forming core–shell hybrid structures. The electron diffraction results revealed that the generated nanoparticles were mainly composed of 3C-SiC@C core shells, which is a novel nanomaterial with promising applications as anode materials for future lithium-ion batteries.

KEYWORDS
carbon, core–shell nanoparticle, laser irradiation, nanomaterial, plume observation, SiC, silicon

1 | INTRODUCTION

In the field of nanomaterials, silicon (Si) and carbon (C) composite nanostructures have attracted considerable interest over the last few years.[1–3] These composites can be used as anode materials in high-performance lithium-ion batteries or lithium-ion capacitors. Recently, there has been an increasing demand for lithium-ion batteries with higher capacity and longer life as quintessential require-ments to achieve a decarbonized society.[4–6] Although graphite is currently used as the manufacturing anode material in lithium-ion batteries, its theoretical capac-ity (370 mAhg^{-1}) is much smaller than that of Si (4200 mAhg^{-1}). Thus, Si has received significant attention as an alternative anode material.[7,8] However, Si anodes have a short lifespan because of their tendency to expand in vol-ume during charging, causing problems such as the shat-tering of the material.[9,10] In addition, the formation of

unstable solid electrolyte interphase layers on Si anodes induces rapid capacity decay.[11]

Using Si/C composite nanostructures is expected to be an effective solution to these problems. Several studies have demonstrated that Si nano-sizing[12–14] and C coating[8,14] can partially resolve the Si expansion problem. It has previously been reported that Si nanoparticles coated with a carbon layer (particularly, Si@C core shell) with a size of 30 nm could provide a reversible lithium insertion capacity of approximately 530 mA hg^{-1} over 100 cycles.[15] Additionally, an earlier study using boron-doped Si@C core–shell nanoparticles as the anode material for lithium-ion capacitors showed a specific energy of 202.5 Whkg^{-1} at 33.135 kWkg^{-1},[16] which was much better than that of conventional lithium-ion capacitors. Therefore, Si@C core–shell nanoparticles enable the widespread use of lithium-ion batteries or lithium-ion capacitors and assist in the decarbonization of our society. Conventionally, Si@C core–shell nanoparticles are produced by forming a C layer on pregenerated Si nanoparticles using substrate-induced coagulation[17] or chemical vapor deposition methods.[8,18] This conventional process consists of two steps, namely, Si nanoparticle generation and C coating, which require a long time and incur a high production cost.

Another alternative is the use of SiC as the anode material. Contrary to Si, SiC can reduce material crushing because of its excellent mechanical properties. SiC was previously considered unsuitable for application as an anode material because of its electrical inertness. However, recent studies have confirmed that 4H-SiC nanoparticles have good charge–discharge properties,[19] and 3C-SiC nanoparticles covered with a graphite film provide a reversible lithium insertion capacity of approximately 1200 mA hg^{-1} over 200 cycles.[20] Coating SiC nanoparticles with a thin layer of carbon is expected to further improve their conductivity.[21]

In this study, we aimed to produce Si/C composite nanoparticles, such as Si@C and SiC@C core–shell nanoparticles, by laser irradiation of a mixture of Si and graphite powders. The proposed method is a single-equipment and single-step process, which can enable the production of Si/C nanostructures in a short time and at a low cost.

Conventionally, single-crystalline Si wafers are used as raw materials for producing Si nanoparticles. Herein we propose the use of waste Si powder as a raw material to generate Si/C core–shell nanoparticles. Waste Si powder is the debris discharged from the grinding or slicing processes of single or polycrystalline Si wafers used for manufacturing solar cells and semiconductor devices. In wafer grinding or slicing, a large portion of the Si material is removed from the wafers or ingots as chips and disposed of as waste,[24] resulting in a significant loss of energy and resources. Sev-

eral researchers have attempted to recycle waste Si powder for ingot production; however, the purification of Si waste remains an obstacle.[25]

In our previous study, we succeeded in producing Si nanostructures like Si nanoparticles[26,27] and nanowires[28] by irradiating waste Si powder with a laser. However, research on the generation of core–shell structures by laser irradiation is still in its infancy, and the process mechanism has yet to be clarified. Moreover, to date, there is no literature on the formation of Si/C core–shell nanomaterial by laser irradiation using Si and C powders as starting materials. Therefore, it is necessary to investigate the plume growth phenomenon of laser irradiation of targets prepared from each powder and the mixed target under different conditions using a high-speed camera. To the best of our knowledge, such observations have not been previously reported. In some studies, Si[22] and C plumes[23] have been photographed independently using a high-speed camera. However, it is difficult to compare the obtained images to elucidate the mechanism of core–shell structure formation because the laser irradiation conditions are distinctly different.

Briefly, this study was aimed at fabricating Si@C and SiC@C core–shell nanoparticles by laser irradiation of a waste Si powder-based mixture to investigate the feasibility of manufacturing anodes for application in high-performance lithium-ion batteries. To elucidate the process mechanism, we investigated the deposition morphology and composition of the products and observed the laser-induced plume generation phenomenon using a high-speed camera. This method can afford an eco-friendly and cost-effective solution for the problems associated with the manufacture of high-performance lithium-ion batteries. Additionally, it can facilitate the fabrication of other novel Si/C-based functional nanomaterials from industrial waste, which contributes to sustainable manufacturing and the realization of sustainable development goals (SDGs).

2 | EXPERIMENTAL METHODS

2.1 | Target preparation

The waste Si powder was obtained by grinding silicon wafers in two stages: rough grinding and fine grinding with a resin- and vitrified-bond diamond wheel, respectively. The waste Si powder had an average grain size of 3.9 μm, which was then mixed with graphite powder with a grain size of 50 μm (Kojundo Chemical Laboratory Co., Ltd., Japan) at a 1:2 (wt%) ratio and mill ground using a pot mill for 3 hours. After the pot milling process, the particle sizes of Si and C were reduced to approximately 1 and
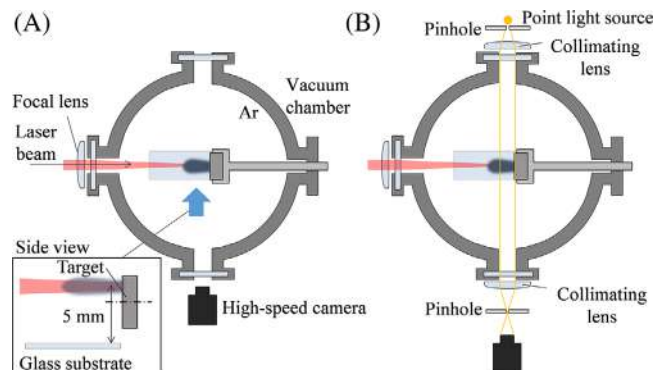
FIGURE 1 Experimental setup for laser irradiation and high-speed camera shooting: (A) top view of the normal high-speed camera setting and (B) top view of camera setting for capturing the schlieren image

20 μm, respectively. Finally, a cylindrical Si/C mixture target with a diameter and height of 1 cm each was prepared by applying a load of 40 kN for 1 minute using a tablet-forming machine.

2.2 | Laser irradiation

A top view of the experimental setup for laser irradiation is shown schematically in Figure 1A. The targets were then placed in a chamber filled with Ar gas, and the pressure in the chamber was set to 0.1 MPa. The laser irradiation was performed using continuous wave laser with a wavelength of 1070 nm and an output power of 390 W. A pulse generator was used to produce a pulsed wave with a pulse width of 10 ms, and irradiation was performed in single-shot mode. The laser beam exhibited a Gaussian energy distribution, which was then focused onto the target surface with a spot diameter of 370 μm.

The expected generation process of nanoparticles by laser ablation is as follows. First, the vaporized material formed a plume when the target was irradiated with a laser beam. As the plume expanded and diffused, it was rapidly cooled by collisions with ambient gas, forming droplets after condensation, which further solidified to form nanoparticles.

2.3 | High-speed camera observation

The generation process of the laser-induced plume was observed in real time using a high-speed camera (FAST-CAM Mini AX50, Photron Ltd., Japan) to investigate the nanoparticle formation mechanism. Because a direct light source was absent within the chamber, the direct camera observation could not capture a clear image of the

plume after laser irradiation. Thus, we used the schlieren method to observe plume dynamics, which is highly sensitive for visualizing density gradients in a plume.[29] When a parallel beam of light passes through an object, the difference in density disturbs the parallel beam, resulting in a nonuniform image known as a schlieren image. Because a point light source is used to create a parallel beam, this method can obtain images without laser emission.

The schlieren image is produced by creating a collimated light with a collimating lens and photographing it with a pinhole placed in front of the light source and the camera, as shown in Figure 1B. The illuminance on the screen is proportional to the first-order gradient of the spatial density of the fluid because the rays passing through the pinhole placed at the focal point of the lens depend on the refractive index of the medium rays in the measurement area.

In these observations, the plume shapes were compared by irradiating Si-only, C-only, and Si/C mixed targets. The Si target was prepared in a manner similar to that of the Si/C mixed target. The C target was also compressed in a tablet press with a small amount of ethanol added for hardening because the particle size of the graphite powder was large and could not be solidified in the same manner as the Si/C mixture. After compression, ethanol was volatilized by natural drying for approximately 20 hours.

2.4 | Nanoparticle characterization

The generated nanoparticles were deposited on a glass substrate, which was placed 5 mm below the target, as shown in the inset side view in Figure 1A. The morphology of the produced nanoparticles was characterized by scanning electron microscopy (SEM, Inspect F50, FEI Company, USA) and transmission electron microscopy (TEM, Tecnai G2 and Tecnai Osiris, FEI Company, USA). The compositions of the nanoparticles were characterized by TEM with a fast Fourier transform (FFT), mapping analysis with energy-dispersive X-ray spectroscopy (EDX) and laser Raman spectroscopy (LabRAM HR Evolution, HORIBA, Ltd., Japan). Multiple single-shot irradiations were performed at different locations to obtain reliable results for the average deposition rates. The irradiation location was changed by rotating the target around its axis. The weight of the deposited nanoparticles was determined by measuring the weight difference between the glass substrate before and after nanoparticle deposition using an electronic balance. The distribution of the deposition thickness was obtained by measuring the cross-sectional profile of the glass substrate with particle deposition using a laser microscope.
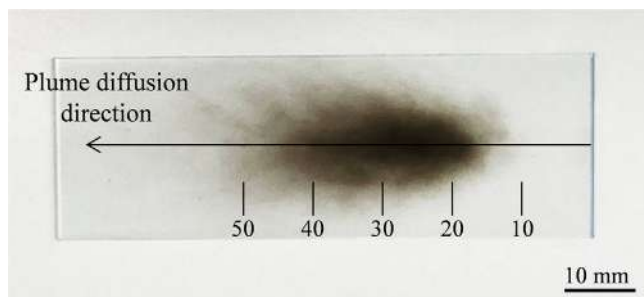
FIGURE 2 Optical image of the deposited nanoparticles on a glass substrate after 30 irradiations

FIGURE 4 Cross-sectional surface profile illustrating the amount of nanoparticles deposited after 10 irradiations

3 | RESULTS AND DISCUSSION

3.1 | Morphology of deposited nanoparticles

Figure 2 shows a photograph of the glass substrate with deposited nanoparticles, which is represented by the dark area. Figure 3 illustrates the SEM images of the nanoparticles located on the glass substrate 10–50 mm distance from the irradiation point. The nanoparticles were deposited at all five locations, and more nanoparticles were deposited closer to the irradiation point. Although the number of deposited particles varied with the scattering distance, the morphology of the deposited particles did not change significantly with the location.

3.2 | Quantity of deposited nanoparticles

The difference in the weight of the glass substrate before and after 10 irradiations was approximately 0.10 mg, indicating that the amount of nanoparticles deposited per irradiation was approximately 0.01 mg. The cross-sectional profiles of the deposited regions on the glass substrate after 10 irradiations are illustrated in Figure 4. Nanoparticles were deposited over a wide area on the glass substrate, beginning approximately 10 mm from the irradi-

FIGURE 3 SEM images of nanoparticles deposited at various locations: at a distance of (A) 10 mm, (B) 20 mm, (C) 30 mm, (D) 40 mm, and (E) 50 mm from the irradiation point
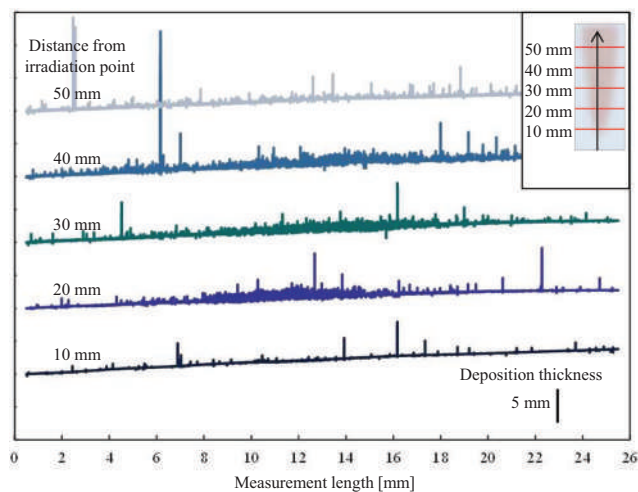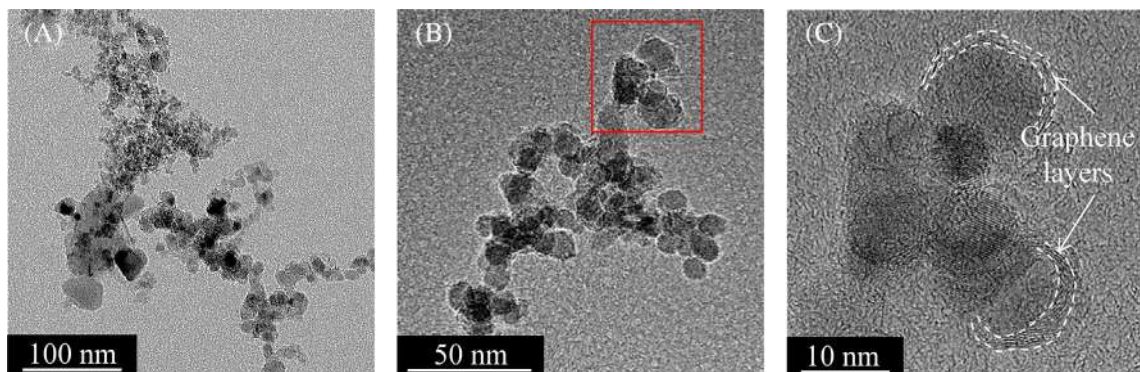
FIGURE 5 TEM images demonstrating the shape and structure of the agglomerated nanoparticles deposited at a distance of 20 mm from the irradiation point, (A) and (B) in full, and (C) is the magnified view of the boxed area in (b)
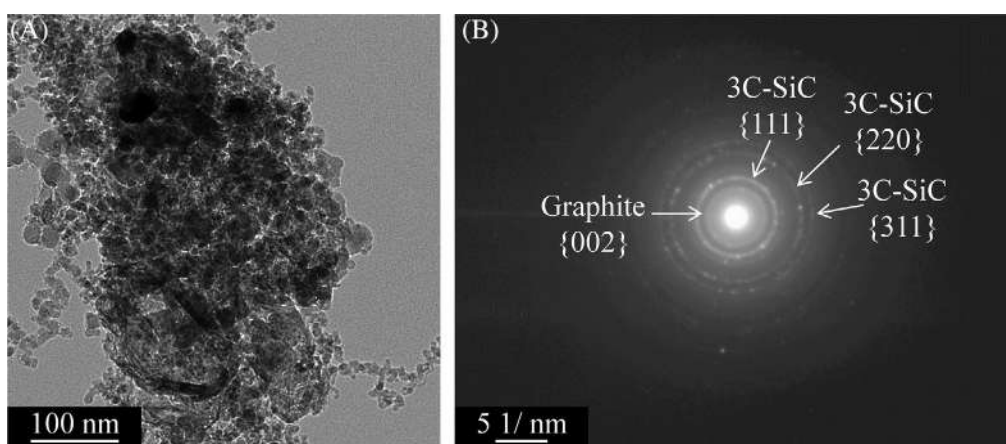

FIGURE 6 (A) TEM image and (B) structural analysis by electron diffraction of nanoparticles in the field of view of (A)

ation point. Most of the nanoparticles were deposited between 20 and 40 mm. However, beyond 40 mm, the deposition height was smaller as the distance was longer.

3.3 | Crystalline structure and composition

The TEM images of the nanoparticles deposited at a distance of 20 mm from the irradiation point are demonstrated in Figure 5. The particle size ranged from a few nm to approximately 40 nm. The TEM image in Figure 5C confirms that the surface of the particles was covered with a layer of graphene. Figure 6A shows a TEM image of a cluster of nanoparticles, and Figure 6B illustrates the electron diffraction pattern of the field of view in Figure 6A, suggesting that the nanoparticles were composed of 3C-SiC and graphite. The shell was composed of multiple layers of graphene; hence, the electron diffraction pattern demonstrated the structure of graphite. Among the polytypes

of SiC, 3C-SiC forms at low temperatures ($\leq$1500°C).[30] Previous studies have reported the formation of 3C-SiC by the laser irradiation of Si wafers in a mixture of Ar and n-heptane at a wavelength of 1064 nm,[31] which is almost similar to the laser wavelength of 1070 nm used in this study. However, the electron diffraction results in Figure 6B do not reveal the existence of Si, which can be attributed to the small amount of Si that cannot be detected using electron diffraction.

Further, EDX mapping was performed to characterize the elemental composition of the deposited nanoparticles, and the results are shown in Figure 7. Few nanoparticles, mapped in light blue (Si), were evenly surrounded by a pink (C) layer. Other nanoparticles were mapped in both light blue and pink, indicating a partial mixture of Si and C or the presence of SiC.

The results of the Raman spectroscopic analysis of nanoparticles are illustrated in Figure 8. The Si peak at 520 cm^{-1} was not observed in the low-wavelength range (Figure 8A), while a graphite peak was observed in the
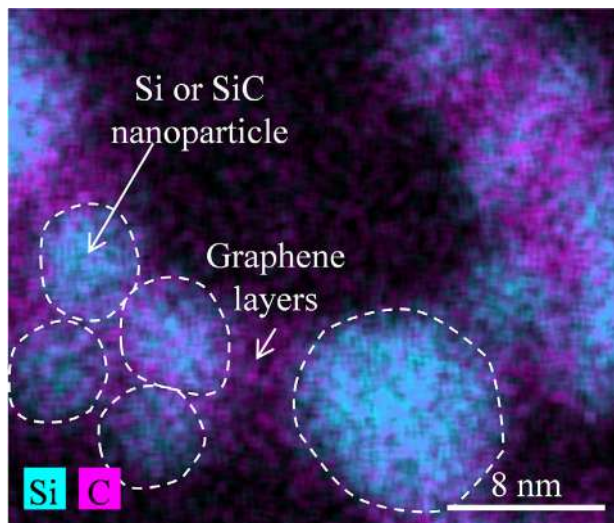
FIGURE 7 EDX mapping analysis image demonstrating the distribution of elements Si and C

high-wavelength range (Figure 8B). The peak at 1360 cm^{-1} (D-band) was attributed to the defects in graphite, and the peak at 1580 cm^{-1} (G-band) was ascribed to the graphite structure. The D-band peak shifted with the wavelength of the laser used in Raman spectroscopy, shifting to a lower wavelength when a long-wavelength laser was used.[32] In the present study, a laser of 633 nm was used in Raman spectroscopy, and the D band shifted to 1325.6 cm^{-1}.

However, the laser Raman spectroscopy results did not show any peaks for Si or SiC. The absence of peaks could be attributed to the high absorbance and short light penetration length of graphite in the visible light region, rendering it difficult to detect internal materials when a graphite layer was formed.[33,34] This result suggested that most of the deposited products were covered by graphite (multilayer graphene), preventing the detection of other materials (Si, SiC). Thus, the result indirectly demonstrates the production of Si@C and SiC@C core–shell nanoparticles

(Si and SiC nanoparticles surrounded by C coatings) during the laser irradiation experiment.

3.4 | Plume observation

The plumes generated by laser irradiation of the Si, C, and Si/C mixed targets were observed using a high-speed camera, and the results are shown in Figure 9. The duration of the plume was longer for the Si target than for the C and Si/C mixed targets. Moreover, the plume of the Si target was scattered as small droplets as time elapsed, whereas the plume of the C target remained continuous without scattering. However, scattered droplets were observed for the plume of the mixed target at the early stage (approximately 3.0 ms) after initiating laser irradiation. Although the droplets were similar to those of the Si-only target, no scattering was observed at the later stage. Furthermore, the plume remained continuous, which was similar to that observed for the C-only target.

The plumes are further investigated from the magnified images of Si and C plumes, as illustrated in Figure 10. Figure 10A shows the light trails of the Si plume droplets. Because the images were captured at 4000 fps, the approximate diffusion velocities of the plume calculated from the light trace lengths indicated in the figure were 4.8, 3.4, 3.8, and 1.8 m s^{-1} at 1, 2, 3, and 4 ms, respectively. However, no evident light trails were observed 8 ms, indicating that the droplets were almost stationary. In addition, a gaseous cloud accompanying the droplet scattering was generated at the lower part of the Si plume, as observed from the magnified images; the gaseous cloud became smaller over time. Conversely, droplet scattering was not observed in the C plume, even in the magnified image (Figure 10B), and only gaseous clouds were observed, which grew gradually as the time elapsed from 1 to 8 ms.

Next, a schlieren image of the Si/C mixed target plume was captured under various conditions. Figure 11 illus-
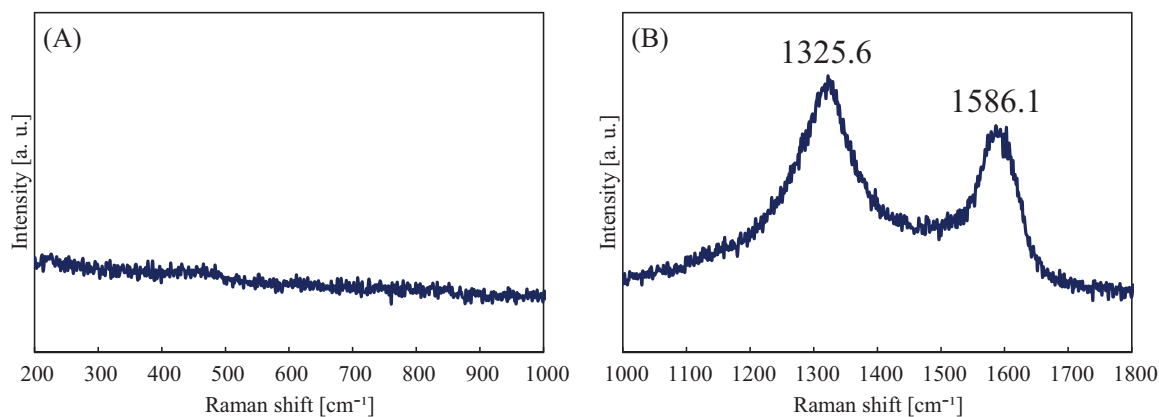

FIGURE 8 Raman analysis of the deposited nanoparticles at (A) low and (B) high wavelength ranges
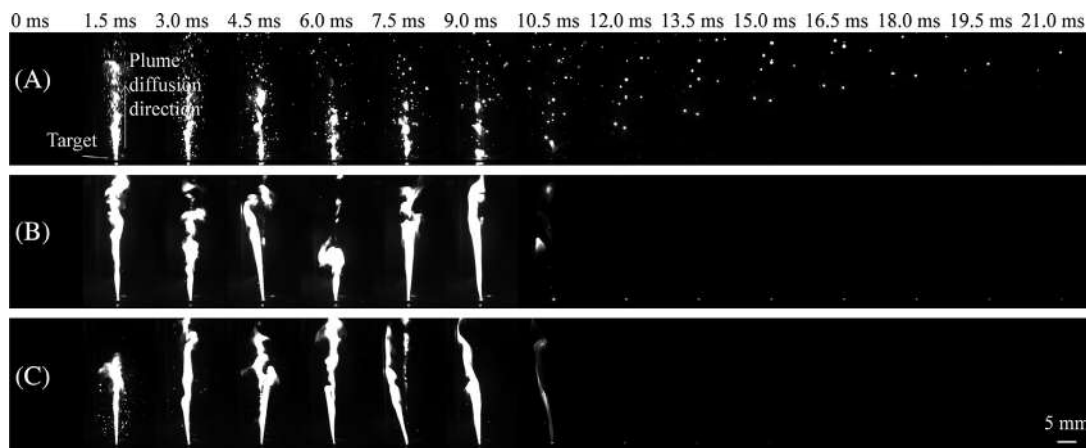
FIGURE 9 High-speed camera images of plume propagation during laser irradiation of (A) Si, (B) C, and (C) Si/C mixed targets

trates the schlieren image of the plume of the Si/C mixed target irradiated by the laser. The plume was generated with an intense change in the plasma density when the laser was irradiated. Notably, the plume was not observed after 10 ms in the normal imaging mode due to the absence of light emission; however, the schlieren image indicated the presence of plasma density fluctuation even after 10 ms. The plasma density fluctuations disappeared after

approximately 15 ms, indicating that the plume remained briefly in the air after laser irradiation and gradually accumulated on the glass substrate. Moreover, the density fluctuations were in the form of a gas rather than in the form of a droplet, suggesting that C gas was the main component.

3.5 | Nanoparticle formation mechanism

Herein, the formation mechanism of Si/C core–shell nanoparticles is discussed from the viewpoints of the nanoparticle composition and plume growth behavior. The predicted nanoparticle formation mechanism is shown schematically in Figure 12. When the Si/C mixed target was irradiated with a laser (Figure 12A), a plume was generated (Figure 12B). The plume contained both small liquid droplets and gaseous plasma clouds (Figure 9B and C at 1.5 ms). The droplets were composed of only Si, and the gaseous plasma cloud was a mixture of Si and C. This observation was proven by the generation of plumes from the Si- and C-only targets, as shown in Figure 9, where the Si plume was composed of droplets and gaseous clouds, whereas the C plume was gaseous. In the droplet plume, Si droplets were cooled and solidified owing to collisions with the ambient gas, forming Si nanoparticles.[35] In the gaseous plume, SiC nanoparticles were formed by collisions and chemical reactions between Si and C atom clusters.[31] As shown in Figure 9C, the plume contained only gaseous clouds at the end of the process for the Si/C mixed target, and the gaseous clouds were mainly composed of C plasma. When Si and SiC nanoparticles passed through the C plasma, the surface of the particles was coated with a C layer (Figure 12C), forming Si@C and SiC@C core–shell nanoparticles. These composite nanoparticles were cooled in ambient gas and finally deposited on a glass substrate (Figure 12D).
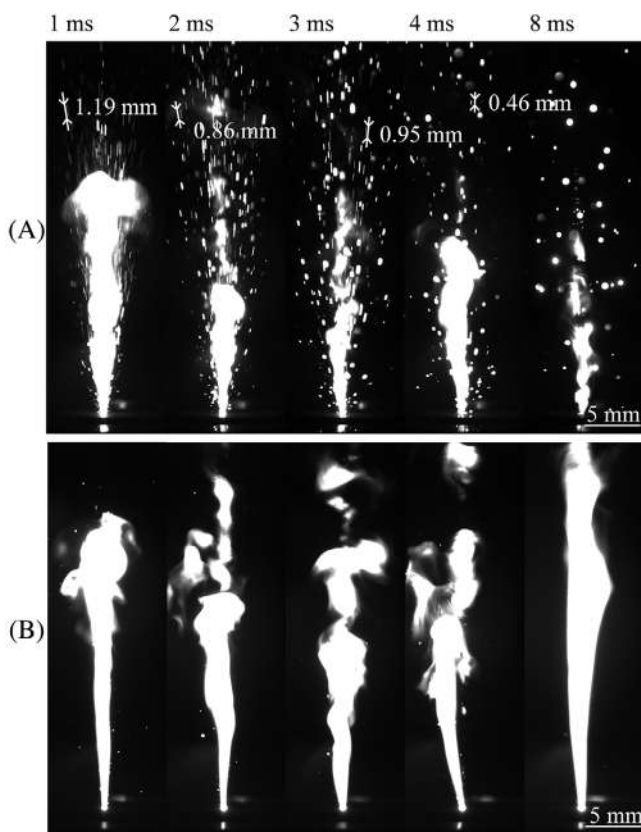

FIGURE 10 Magnified high-speed camera images of plume propagation of (A) Si and (B) C targets
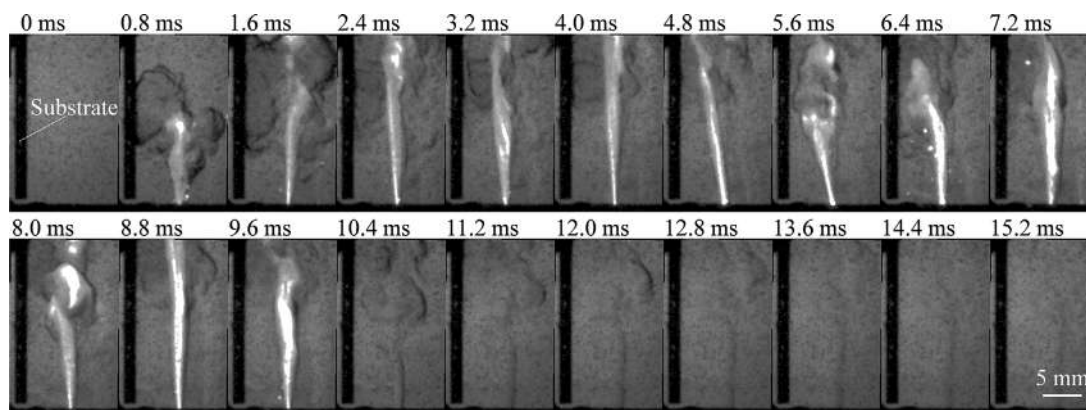
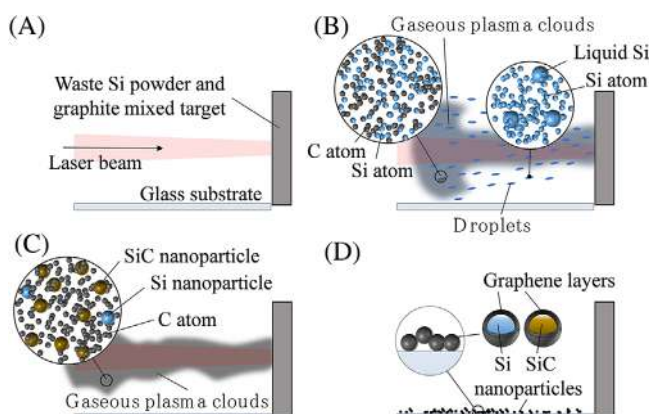**FIGURE 11** Schlieren image of the plume from inception to extinction for the Si/C mixed target

FIGURE 12 Schematic of the mechanism of Si/C composite nanoparticle formation: (A) laser irradiation, (B) plume generation, (C) nanoparticle formation in the plume, and (D) cooling and deposition

4 | CONCLUSIONS

In this study, a mixture of waste Si and graphite powders was irradiated with a laser to generate Si@C and SiC@C core–shell nanoparticles. The morphology, quantity, crystalline structure, and composition of the nanoparticles as well as the laser-induced plume diffusion behavior were investigated. The primary conclusions are as follows:

- Si/C composite nanoparticles were successfully generated in a single-step process by laser irradiation of a mixture of waste Si and graphite powders. The main product of this process is 3C-SiC@C core–shell nanoparticles.
- Most products were deposited on a glass substrate at a distance of 10 to 20 mm from the target surface. The size of the generated nanoparticles ranged from a few nanometers to 40 nm, which did not change with increasing distance from the target surface.

- The shape and time characteristics of the plume for the Si target were different from those of the C target. This difference enabled the formation of core–shell hybrid structures during the laser irradiation process.
- When Si and SiC nanoparticles generated in the early stage passed through the C plasma remaining at the late stage, the surfaces of the particles were coated with C layers, forming Si@C and SiC@C core–shell nanoparticles.

The results of this study provide an eco-friendly and cost-effective solution for manufacturing high-performance anodes for future lithium-ion batteries from industrial waste. By changing the laser irradiation conditions and the composition of the target materials, the proposed method provides the possibility of creating new types of Si/C-based functional nanomaterials, which is also a future task of our research. The success of research in this direction can contribute to sustainable manufacturing and industrial symbiosis, thereby realizing SDGs.

DATA AVAILABILITY STATEMENT
Data sharing is not applicable to this article as no new data were created or analyzed in this study.

ORCID
Jiwang Yan https://orcid.org/0000-0002-5155-3604

REFERENCES

1. X. Lv, W. Wei, B. Huang, Y. Dai, *J. Mater. Chem. A* **2019**, *7*, 2165.
2. L. Chen, X. Xie, B. Wang, K. Wang, J. Xie, *Mater. Sci. Eng. B: Solid-State Mater. Adv. Technol.* **2006**, *131*, 186.
3. S. Cui, S. Chen, L. Deng, *Ceram. Int.* **2020**, *46*, 3242.
4. J. B. Goodenough, Y. Kim, *Chem. Mater.* **2020**, *22*, 587.
5. M. Armand, J.-M. Tarascon, *Nature* **2008**, *451*, 652.
6. J. Chen, F. Cheng, *Acc. Chem. Res.* **2009**, *42*, 713.
7. H. Wu, G. Yu, L. Pan, N. Liu, M.T. McDowell, Z. Bao, Y. Cui, *Nat. Commun.* **2013**, *4*, 1943.
8. L. Hou, H. Zheng, R. Cui, Y. Jiang, Q. Li, X. Jiang, J. Gao, F. Gao, *Microporous Mesoporous Mater.* **2019**, *275*, 42.
9. X. Xiao, P. Liu, M. W. Verbrugge, H. Haftbaradaran, H. Gao, *J. Power Sources*, **2011**, *196*, 1409.
10. L. Y. Beauliu, K. W. Eberman, R. L. Turner, L. J. Krause, J. R. Dahna, *Electrochem. Solid-State Lett.* **2001**, *4*, A137.
11. H. Wu, G. Chan, J. W. Choi, I. Ryu, Y. Yao, M. T. Mcdowell, S. W. Lee, A. Jackson, Y. Yang, L. Hu, Y. Cui, *Nat. Nanotechnol.* **2012**, *7*, 310.
12. M. T. McDowell, S. W. Lee, W. D. Nix, Y. Cui, *Adv. Mater.* **2013**, *25*, 4966.
13. J. O. Besenhard, J. Yang, M. Winter, *J. Power Sources* **1997**, *68*, 87.
14. J. Liu, P. Kopold, P. A. vanAken, J. Maier, Y. Yu, *Angew. Chem. Int. Ed.* **2015**, *54*, 9632.
15. B. Liu, H. Lu, G. Chu, F. Luo, J. Zheng, S. Chen, H. Li, *Chin. Phys. B* **2018**, *27*, 088201.
16. X. Dai, S. Lei, J. Liu, Z. Shang, S. Zhong, X. Li, *J. Power Sources.* **2021**, *498*, 229912.
17. Y. Hwa, W.-S. Kim, S.-H. Hong, H.-J. Sohn, *Electrochim. Acta*, **2012**, *7*, 201.
18. J. Yu, J. Yang, X. Feng, H. Jia, J. Wang, W. Lu, *Ind. Eng. Chem. Res.* **2014**, *53*, 12697.
19. H. Zhang, H. Xu, *Solid State Ionics* **2014**, *263*, 23.
20. T. Sri Devi Kumari, D. Jeyakumar, T. Prem Kumar, *RSC Adv.* **2013**, *3*, 15028.
21. F. Huang, S. Fan, X. Li, X. Qu, Y. Tian, X. Zhang, Z. Zhang, X. Dong, T. Cao, *Nanotechnology* **2021**, *32*, 265705.
22. T. Hirata, Z. Miyazaki, *Anal. Chem.* **2007**, *79*, 147.
23. S. Suzuki, R. Sen, T. Tamaki, H. Kataura, Y. Achiba, *Eur. Phys. J. D* **2003**, *24*, 401.
24. D. Sarti, R. Einhaus, *Sol. Energy Mater. Sol. Cells* **2002**, *72*, 27.
25. H. D. Jang, H. Kim, H. Chang, J. Kim, K. M. Roh, J.-H. Choi, B.-G. Cho, E. Park, H. Kim, J. Luo, J. Huang, *Sci. Rep.* **2015**, *5*, 9431.
26. K. Momoki, J. Yan, *Appl. Phys. Express* **2020**, *13*, 026505.
27. K. Momoki, T. Manabe, L. Li, J. Yan, *Mater. Sci. Semicond. Process.* **2020**, *111*, 104998.
28. K. Momoki, K. Takahashi, K. Kobinata, Y. Kobayashi, A. Kawai, J. Yan, *Nanomaterials* **2020**, *10*, 812.
29. I. B. Gornushkin, U. Panne, *Spectrochim. Acta, Part B.* **2010**, *65*, 345.
30. H. Matsunami, T. Kimoto, *Mater. Sci. Eng. R Rep.* **1997**, *20*, 125.
31. K.-M. Lv, J. Yang, K.-Y. Niu, H.-L. Wang, J. Sun, X.-W. Du, *Mater. Lett.* **2009**, *63*, 2492.
32. Y. Wang, D. C. Alsmeyer, R. L. McCreery, *Chem. Mater.* **1990**, *2*, 557.
33. X. Yang, J. Qin, Y. Li, R. Zhang, H. Tang, *J. Hazard. Mater.* **2013**, *261*, 342.
34. J. Zang, L. Dong, Y. Jia, H. Pan, Z. Gao, Y. Wang, *Appl. Catal., B* **2014**, *144*, 166.
35. F. Kokai, S. Inoue, H. Hidaka, K. Uchiyama, Y. Takahashi, A. Koshio, *Appl. Phys. A: Mater. Sci. Process.* **2013**, *112*, 1.